CHAPTER 3

EXPERIMENTAL PROCEDURE

3.1 Chemical reagents, and instruments

3.1.1 Chemical reagents

1) Tellurium powder, Te, M.W. = 127.60, purum, analytical grade, Fluka
2) Zinc powder, Zn, M.W. = 65.39, purum, analytical grade, Fluka
3) Antimony powder, Sb, M.W. = 121.76, purum, analytical grade, M&B
4) Bismuth powder, Bi, M.W. = 208.98, purum, analytical grade, Merck
5) Nickel chunk, Ni, M.W. = 58.69, 3N, Fine Chemical
6) Gallium antimonide chunk, GaSb, M.W. = 191.438, 5N, Fine Chemical
7) Indium antimonide chunk, InSb, M.W. = 236.578, 6N, Fine Chemical
8) Argon gas, Ar, M.W. = 39.948, > 99.9 %, TIG

3.1.2 Instruments

1) Analytical balance, model BP-210S, Sartorius AG. Goettingen, Germany
2) Microwave oven, Electrolux model 2820S
3) Scanning Electron Microscope, and Energy Dispersive X-ray Spectroscopy, model JEM-6335, JEOL, Japan
4) Scanning Electron Microscope and Energy Dispersive X-ray Analyser, model S2600H, Hitachi, Japan
5) Transmission Electron Microscope, model JEM-2010, JEOL, Japan

6) X-ray Diffractometer, model Xpert MPD, Philips, Netherlands
7) X-ray Diffractometer, model RINT, Rigaku, Japan
8) X-ray Diffractometer, model D8 Advance, Bruker
9) Raman spectrophotometer, model T64000 JY, Horiba Jobin Yvon, France
10) Luminescence spectrometer, model LS50B, Perkin Elmer
11) UV-Vis-NIR spectrophotometer, model Lambda 19, Perkin Elmer
12) Spark plasma sintering machine, model SPS-515A, Syntex, Japan
13) Seebeck Coefficient/Electric Resistance Measuring System, ZEM-1, ULVAC, Japan
14) Hall effect measurement system, model ResiTest 8300, Toyo technical
15) Laser Flash Thermal Constants Analyzer, TC-7000, ULVAC, Japan

3.2 Synthesized methods

3.2.1 Synthesis of ZnTe using microwave plasma

To produce ZnTe, Zn and Te powders (purum, analytical grade, Fluka) were used without further purification. Two solid mixtures with 1:1, 1.5:1 and 1.8:1 molar ratios of Zn:Te (2 g each) were loaded into silica tubes (11 mm I.D. x 100 mm long), each of which was placed in a horizontal (H) quartz tube (Figure 3.1). The tube was tightly closed and evacuated to 4.3±1 kPa absolute pressure for removal of air. Subsequently, argon was gradually fed into this H tube. The procedure was repeated three times. Finally, argon in the H tube was evacuated to a constant value of 4.3±1 kPa absolute pressure. Simultaneously, each solid mixture was heated by a 900 W

microwave plasma for 10 min, and left cool down in the vacuum to room temperature. The solid was milled and thoroughly mixed for 5 min. Microwave heating was repeated under the same condition for 10 min at a time, until at the completion of the process. The microwave was heated the sample of 1:1, and 1.5:1 molar ratio products for 10, 20, 30 and 40 min, and 1.8:1 molar ratio products for 10 and 20 min, respectively. They were then characterized to determine their phase, morphologies, vibrations and emission.

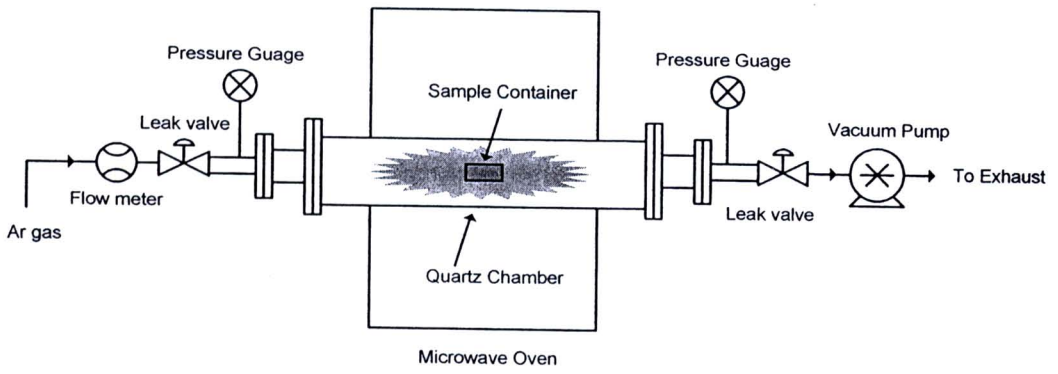

Figure 3.1 Schematic diagram of microwave induced plasma system.

3.2.2 Synthesis of Sb_2Te_3 using microwave plasma

Sb and Te powders (purum, analytical grade, Fluka) for the present synthesis were used without further purification. Different molar ratios of Sb:Te (2:3, 2:2, 2:1.75, and 2:1.5) were loaded into 11 mm I.D. x 100 mm long silica tubes. Each was placed in a horizontal (H) quartz tube (Figure 3.1), which was tightly closed and evacuated to 4.3±1 kPa absolute pressure. Argon was gradually fed into this H tube. Evacuation was repeated three times. Finally, each solid mixture was heated by a 900 W irradiated microwave plasma for 10 and 20 min in 4.3±1 kPa absolute pressure,

and left to cool down to room temperature. The products were then characterized to determine their phase, morphologies, vibrations and optical property.

Products were characterized and recorded on a Philips X'Pert MPD X-ray diffractometer (XRD) equipped with a graphitic monochromator of Cu K_α radiation (λ = 0.154056 nm), using a scanning rate of 0.02 deg/s over the 2θ range of 10° - 60°. Raman vibrations of the products were detected by a HORIBA JOBIN YVON T64000 Raman spectrometer with 30 mW and 632.8 nm (red) wavelength He-Ne laser. Field-emission scanning electron microscopic (FESEM) image was taken by a JEOL JSM-6335F operated at 15.0 kV beam energy. Transmission electron microscopic (TEM) images, and selected area electron diffraction (SAED) patterns were taken on a JEOL JEM-2010, employing at an accelerating voltage of 200 kV. Ultraviolet (UV)-visible spectra were carried out by a Lambda 25 spectrometer using UV lamp with the resolution of 1 nm at room temperature.

3.2.3 Synthesis of Ni_3GaSb and Ni_3InSb using alloying preparation in a furnace

The Ni_3GaSb and Ni_3InSb ternary compounds were synthesized by direct reactions of mixtures of the stoichiometric ratios of Ni (3N), GaSb (6N), and InSb (5N) in sealed silica tubes. These mixtures were processed in a series of steps: preheated at 973 K for 12 h, slowly heated up to 1323 K for 3 days, rapidly cooled to 973 K and held at this temperature for 4 days, and quenched in an ice water bath. The products were crushed and milled into fine powders. Bulk samples were then produced by spark plasma sintering (SPS-515A, Syntex) of the fine powders in a 20 mm diameter graphite die using 40 MPa sintering pressure at 1123 K for 30 min in an

argon-flow atmosphere as shown in Figure 3.2 The ingots were cut into the rectangular shapes of 3 mm × 3 mm × 15 mm, and 10 mm × 10 mm × 1 mm. Their phases, morphologies, and chemical compositions were characterized by a powder X-ray diffraction (XRD) technique using Cu Kα radiation in a step scan condition (fixed time) with an increment of 0.02° and a slit-condition of 1.0°-1.0°-0.60 mm (DS-SS-RS) on Rigaku RINT 2000, and a scanning electron microscope (SEM) equipped with an energy dispersive X-ray (EDX) analyzer (Hitachi, S2600H) at room temperature. The density of the bulk samples was calculated based on the measured weight and dimensions. The electrical resistivity (ρ) and the Seebeck coefficient (α) were measured using a commercially available apparatus (ULVAC, ZEM-1) in a helium atmosphere. Thermal conductivity (κ) was evaluated from thermal diffusivity (κ_{dif}), heat capacity (C_p) and sample density (d) based on the relationship $\kappa = \kappa_{dif} C_p d$. The thermal diffusivity was measured under vacuum by the laser flash apparatus (ULVAC, TC-7000). C_p was estimated from the Dulong-Petit model, $C_p = 3nR$, where n is the number of atom per formula unit and R is the gas constant. The TE properties were evaluated in the temperature range from room temperature to 1073 K.

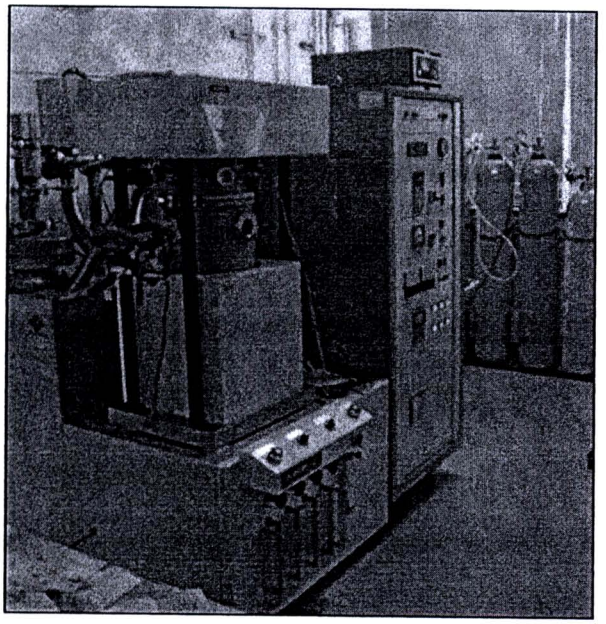

Figure 3.2 Spark plasma sintering machine, model SPS-515A, Syntex, Japan.

3.3 Characterization

This section describes the characterization techniques on the samples in term of phases, chemicals, morphologies, microstructures, optical properties, and thermoelectric properties.

3.3.1 X-ray diffraction (XRD)

Crystalline degree and phase purity of the products were analyzed by X-ray diffractometer (XRD) with Cu K_α radiation (λ = 0.154056 nm) operating at 20 kV-15 mA, at a scanning rate of 0.04°/s in the 2θ range of 10° - 120° (Figure 3.3). The products were specified by a Philips X'Pert HighScore Computer Software (search-match program) of the JCPDS database.

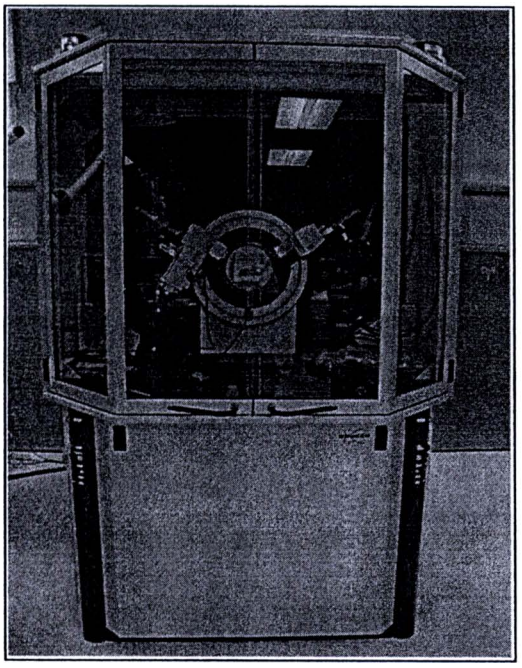

Figure 3.3 X-ray diffractometer.

3.3.2 Scanning electron microscope (SEM) and energy dispersive X-ray analyser

The morphology and particle sizes of the as-synthesized samples were determined by a field emission-scanning electron microscope (FESEM, JSM-6335F) operated at 15 kV accelerating voltage as shown in Figure 3.4 (a), and a scanning electron microscope (S2600H, Hitachi) as shown in Figure 3.4 (b). The chemical compositions were investigated by energy dispersive X-ray (EDX) analyzer equipped to SEM and controlled by Inca program.

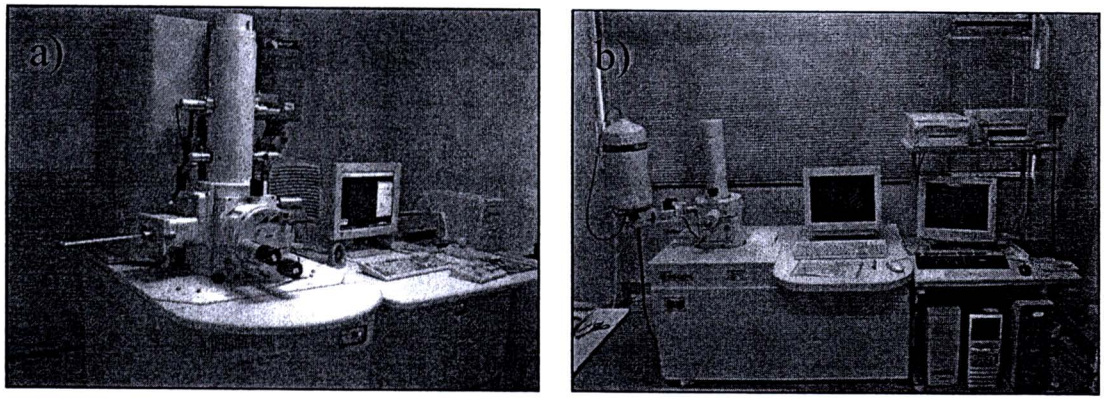

Figure 3.4 (a) Field emission-scanning electron microscope and (b) Scanning electron microscope.

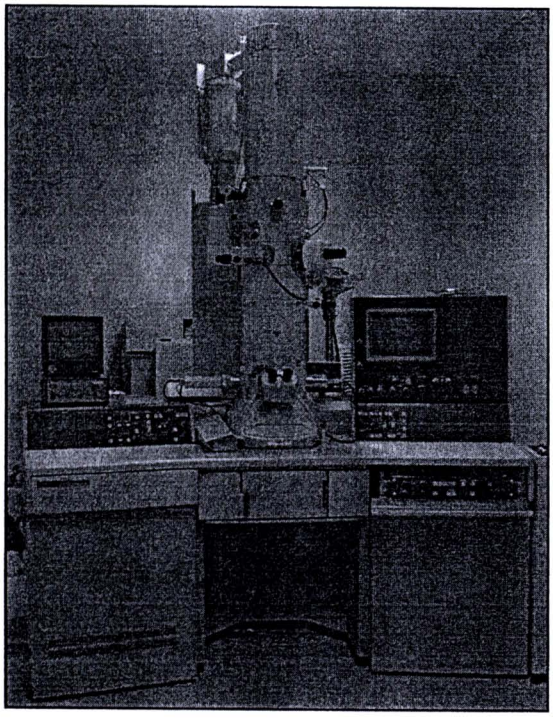

Figure 3.5 Transmission electron microscope.

3.3.3 Transmission electron microscope (TEM)

The particle size and morphology were also characterized by transmission electron microscope (TEM, JEOL JEM-2010) operating at 200 kV as shown in Figure 3.5. The samples for TEM analysis were prepared by dispersing small amount of the powders in absolute ethanol and dropping of the solutions on copper grids coated with holey carbon films, and leaving the ethanol evaporate slowly in air.

3.3.4 Luminescence spectrometer

The luminescence emission spectra of the samples were investigated using Perkin Elmer Luminescence Spectrometer LS50B (Figure 3.6) at room temperature.

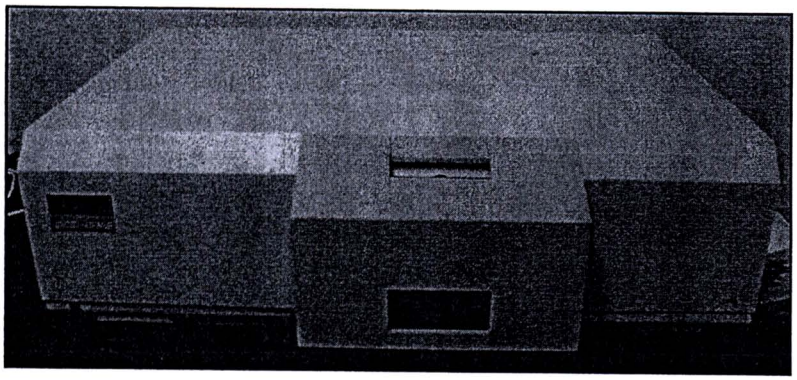

Figure 3.6 Luminescence spectrometer.

3.3.5 UV-Vis-NIR spectrophotometer

The transmission and absorption spectra of the samples were investigated using UV-Vis-NIR Spectrophotometer, model Lambda 19, Perkin Elmer (Figure 3.7) at room temperature. The optical property of the sample was studied using UV-Vis-NIR spectrophotometer with the aid of the following equations [69]:

$$(\alpha_{abs}hv) = A(hv - E_g)^n \quad (3.1)$$

$$\alpha_{abs} = -(\log T)/t \quad (3.2)$$

$$t = bC/d \quad (3.3)$$

where α_{abs} is the total absorption coefficient, hv is the photon energy, A is a constant, E_g is the energy gap, n is a pure number associated with the different types of electronic transitions: n = 1/2, 2, 3/2 or 3 for direct-allowed, indirect-allowed, direct-forbidden and indirect-forbidden transitions, respectively. T is the transmittance of photon through the suspension in ethanol (concentration, $C = 0.001$ g/cm^3) containing in the cuvettes (spectroscopy cells) with the path length (b) of 10.00 mm, t is the effective thickness, and d is the density of sample. The curves of $(\alpha_{abs}hv)^2$ vs (hv) for direct allowed transition were plotted, and extrapolated to $\alpha_{abs} = 0$. The absorption edge energies, corresponding to the energy gap of the samples.

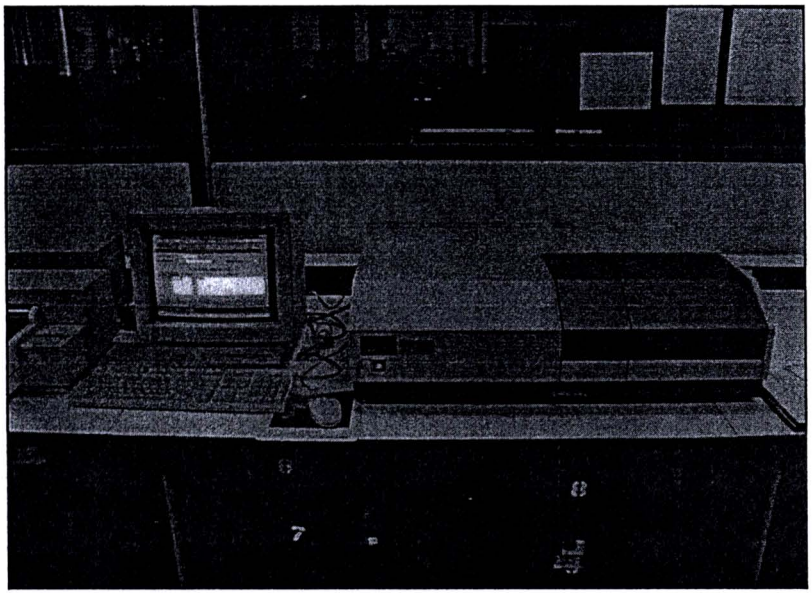

Figure 3.7 UV-Vis-NIR Spectrophotometer.

3.3.6 Raman spectrometer

The Raman instrument provides a powerful tool for the definite identification and characterization of minerals and biomarkers. Raman spectroscopy is sensitive to the composition and structure of any mineral or organic compound. This capability provides direct information of potential organic compounds that can be related with present or past signatures of life on Mars as well as general mineralogical information for igneous, metamorphous, and sedimentary processes, especially water-related geo-processes. The T64000 Raman spectrometer triple monochromator with 30 mW and 632.8 (red) wavelength He-Ne laser of Jobin Yvon Horiba was used to investigate the pure phase of the samples as shown in Figure 3.8.

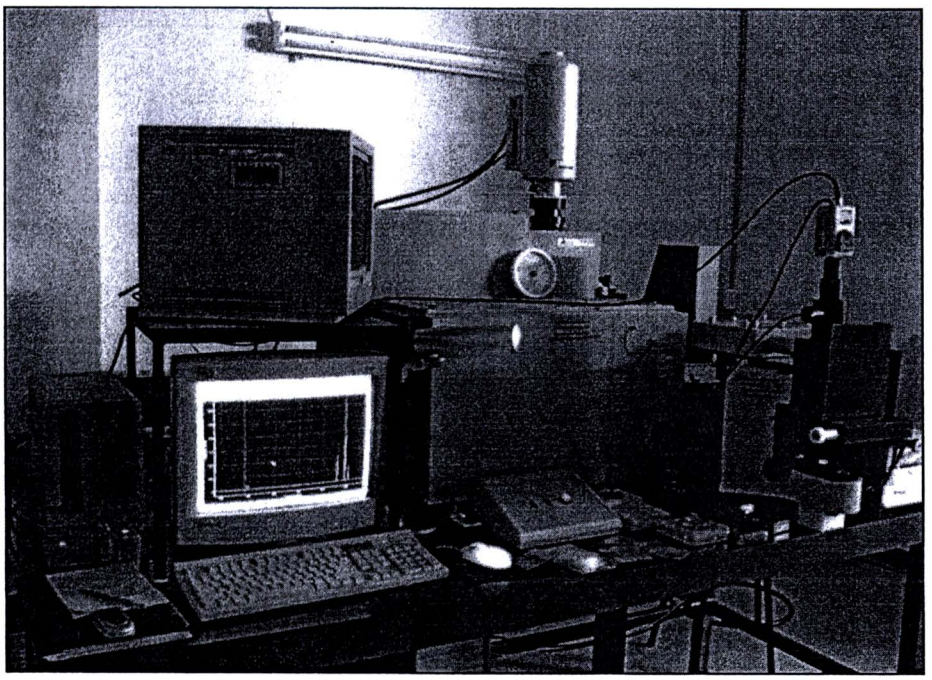

Figure 3.8 Raman spectrometer.

3.3.7 Seebeck coefficient/electrical resistance measuring system

Thermoelectric power is essential to evaluate the performance of the thermoelectric Seebeck coefficient. Seebeck Coefficient/Electrical Resistance Measuring System (Figure 3.9) is a device for simultaneous measurement of both Seebeck coefficient and electrical resistance (resistivity) under an inert gas atmosphere. The instrument permits measurement of both 6-22 mm long prism and cylindrical samples. The sample holder used as a unique balance contact mechanism, permitting measurement of high reproducibility. *V-I* plots were made to judge if the lead is in intimate contact with a set sample. Measurement was controlled by a computer, permitting automatic measurement with each temperature difference at a specified temperature and elimination of dark electromotive force. Temperature range was able to be raised from room temperature to 800°C. A number of measurement temperature steps and sample temperature difference steps were at a maximum of 125°C.

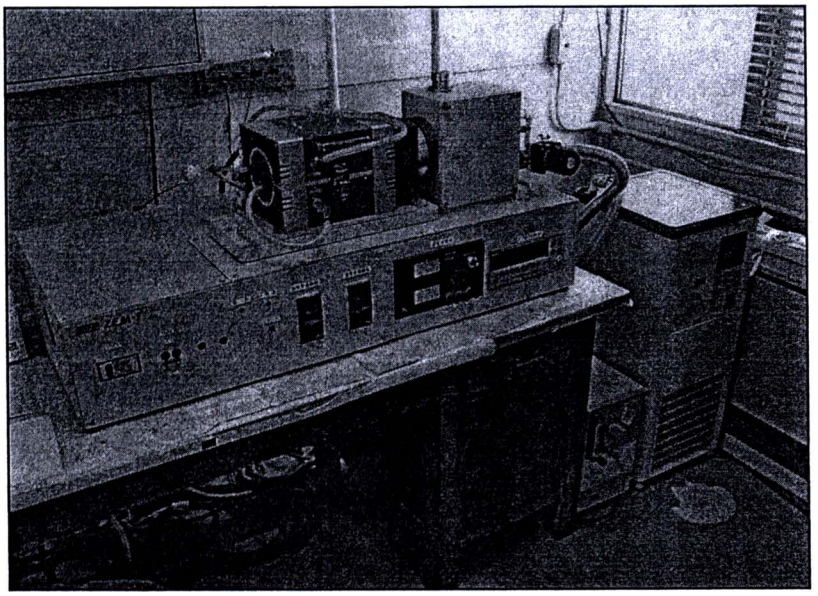

Figure 3.9 Seebeck Coefficient/Electrical Resistance Measuring System.

3.3.8 Hall effect measurement system

The importance of the Hall effect was needed to determine accurately carrier density, electrical resistivity, and the mobility of carriers in semiconductors. The objective of the Hall measurement in the van der Pauw technique was to determine the sheet carrier density n_s by measuring the Hall voltage V_H. The Hall voltage measurement consisted of a series of voltage measurements with a constant current I, and a constant magnetic field B applied perpendicular to the plane of the samples. Conveniently, the samples showed in Figure 3.10, were also used for the Hall measurement. To measure the Hall voltage V_H, a current I was forced through the opposing pair of contacts 1 and 3 and the Hall voltage V_H (= V_{24}) was measured across the remaining pair of contacts 2 and 4. Once the Hall voltage V_H was acquired, the sheet carrier density n_s was able to be calculated via $n_s = IB/q|V_H|$ from the known values of I, B, and q (where q was the elementary charge, 1.602×10^{-19} coul.). The Hall coefficient (R_H) at room temperature was measured by the van der Pauw method in vacuum under 0.5 T applied magnetic field (Toyo technical, ResiTest 8300) as shown in Figure 3.12. The Hall carrier concentration ($n_H = 1/eR_H$) and Hall mobility ($\mu_H = R_H/\rho$) were then calculated from R_H, assuming a single band model and a Hall factor of 1 with e the elementary electronic charge. Figure 3.11 shows Hall effect measurement system of model ResiTest 8300, Toyo technical, Japan.

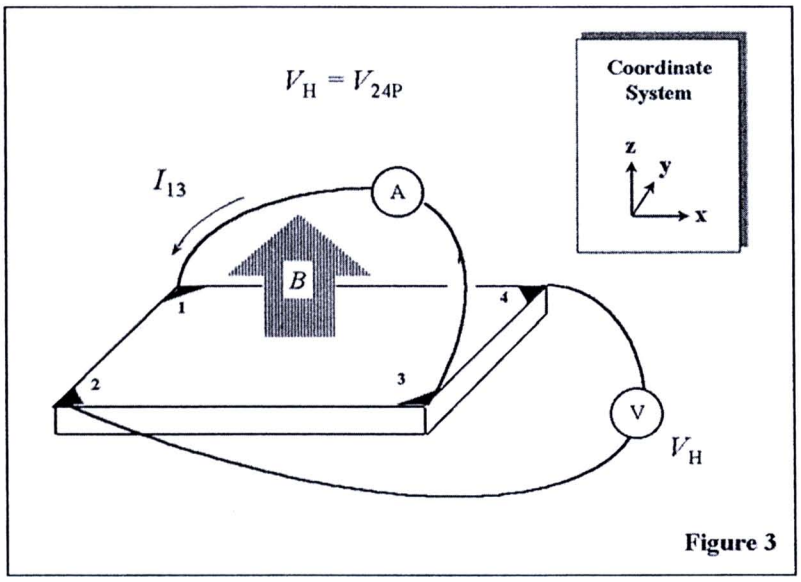

Figure 3.10 Schematic of a van der Pauw configuration used for the determination of Hall voltage V_H.

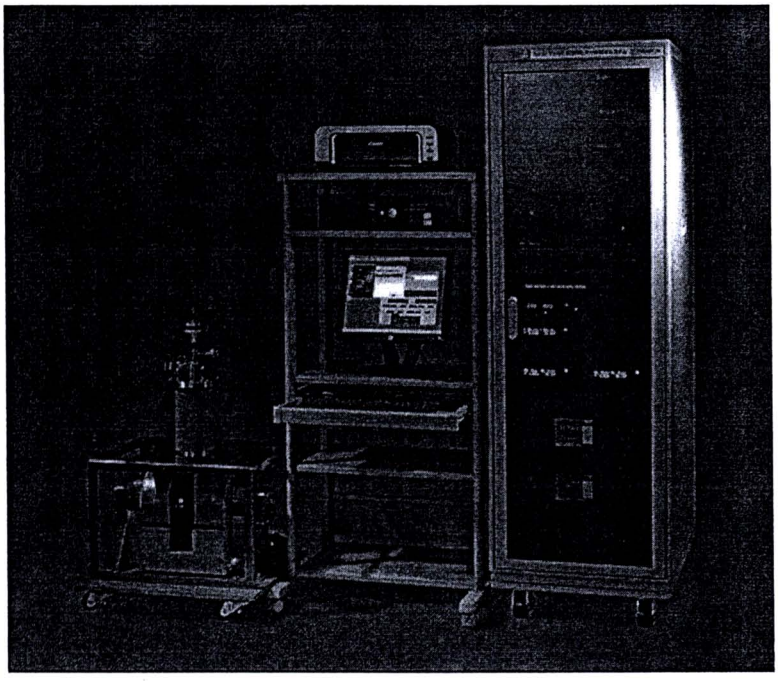

Figure 3.11 Hall effect measurement system.

3.3.9 Laser flash thermal constant analyzer

ULVAC-RIKO system makes the difference in research and development and quality control of high-tech materials. ULVAC-RIKO's system is a widely accepted Laser Flash method to measure three thermal constants: thermal conductivity, thermal diffusivity, and specific heat. Since 1970, ULVAC-RIKO has delivered over 300 laser thermal constant measuring units around the world. Now ULVAC-RIKO presents its most advanced laser thermal constant measuring system: the TC-7000. Thermal conductivity (κ) was calculated from thermal diffusivity (κ_{dif}), heat capacity (C_p), and sample density (d) based on the relationship $\kappa = \kappa_{dif} C_p d$. The κ_{dif} was measured under vacuum using the laser flash apparatus (ULVAC, TC-7000) as shown in Figure 3.12. C_p was estimated from the Dulong-Petit model, $C_p = 3nR$, where n is the number of atom per formula unit, and R is the gas constant.

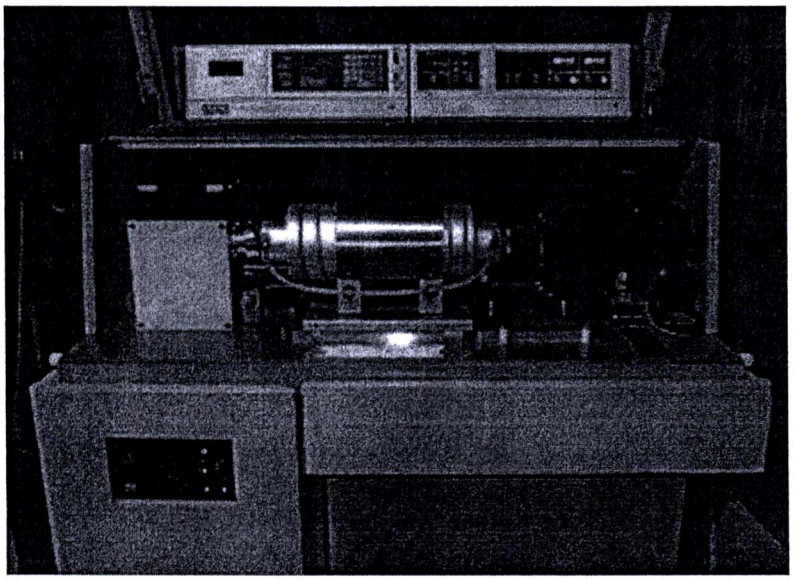

Figure 3.12 Laser Flash Thermal Constant Analyzer.